ACS OMEGA

Open Access

http://pubs.acs.org/journal/acsodf

Article

Esterified Indole-3-propionic Acid: A Novel Inhibitor against Cholinesterase Identified through Experimental and Computational Approaches

Jayanthi Sidhambaram, Penislusshiyan Sakayanathan, Chitra Loganathan, Ancy Iruthayaraj, and Palvannan Thayumanavan*

Cite This: *ACS Omega* 2025, 10, 9073−9087

Read Online

ACCESS | Metrics & More | Article Recommendations | Supporting Information

ABSTRACT: Acetylcholinesterase (AChE) and butyrylcholinesterase (BChE) are targeted for designing drugs against cognitive dysfunction. Curcumin (CUR) and indole-3-propionic acid (IPA) are known for their neuroprotective activity. The clinical application of CUR is hindered due to poor absorption and bioavailability. Hence, CUR was conjugated with IPA to form the CUR-IPA diester. CUR-IPA inhibition against electric eel AChE (eAChE), human AChE (hAChE), and hBChE was carried out. In silico and molecular dynamics (MD) analyses of the interaction of CUR-IPA with hAChE and hBChE were done. UV−visible spectroscopy (λ_{max} at 415 and 276 nm), NMR spectrum, and ESI/MS/MS [m/z = 711 (M + H)] confirmed CUR-IPA formation. CUR-IPA showed in vitro antioxidant activity. The IC_{50} values of eAChE, hAChE, and hBChE enzyme inhibition were 5.66, 59.30, and 60.66 μM, respectively. MD simulation-based analysis such as RMSD, RMSF, free-energy calculation, PCA, FEL, and DCCM confirmed the stable binding of CUR-IPA with hAChE and hBChE. Further QM/MM analysis confirmed the stable interaction of CUR-IPA with hAChE and hBChE. Since CUR-IPA showed in vitro inhibition against AChE and BChE, a further neuroprotective effect in in vivo could be studied.

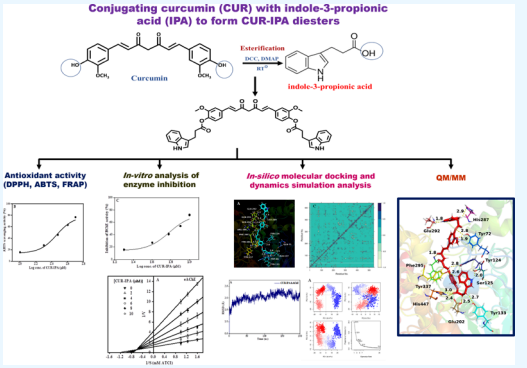

1. INTRODUCTION

Alzheimer's disease (AD) is a neurological disorder which is characterized by altered memory and learning function.[1] According to World Health Organization report, at present 55 million people have dementia worldwide, and AD may contribute to 60−70% of the cases (www.who.int). Clinical and pathological signs of AD include neuronal degeneration, oxidative stress, accumulation of amyloid β (Aβ) plaques, formation of neurofibrillary tangles, and decrease of cholinergic neurotransmitter [acetylcholine (ACh)].[2−5] The cholinergic hypothesis is the most widely studied hypothesis under AD conditions. The hypothesis suggests that at the early stage of AD progression, cognitive impairment is correlated with a loss of cholinergic innervation in the cerebral cortex of AD patients.[6] Cholinesterase (ChE) enzymes acetylcholinesterase (AChE) and butyrylcholinesterase (BChE) are involved in cholinergic neurotransmission through hydrolysis of ACh. Hence, AChE and BChE have been targeted for the symptomatic treatment of AD. The drugs approved for AD are mostly inhibitors of these enzymes.[7] AChE and BChE have been found to be associated with Aβ plaques and neurofibrillary tangles in the brain. Also, these enzymes are reported to be involved in Aβ peptide fibril assembly and its maturation.[8−11] Oxidative stress is another pathological sign that highly impacts the progression of AD.[12] Aβ-induced oxidative stress leads to neurotoxicity which stimulates the progression of AD.[13] Hence, to prevent the pathological severity of AD, it is necessary to design drugs which act on AD-associated risk factors such as oxidative stress and cholinergic enzyme (AChE and BChE) activity. At present, AChE inhibitors, rivastigmine, donepezil, and galantamine, have been approved for the treatment of AD.[14] However, clinically approved inhibitors for AChE possess undesirable side effects such as gastrointestinal abnormalities, hepatotoxicity, nausea, diarrhea, vomiting, agitation, weight loss, stomach upset, skin rash, and chills.[15] Therefore, the search for safer and effective new drug molecules is mostly appreciated.

Curcumin (CUR) (diferuloylmethane or 1,7-bis(4-hydroxy-3-methoxyphenyl)-1,6-heptadiene-3,5-dione) is a potent polyphenolic compound derived from turmeric (*Curcuma longa*). The biological property of CUR includes antioxidant, antimicrobial, anticancer, anti-inflammatory, neuroprotective,

Received: September 4, 2024
Revised: October 28, 2024
Accepted: February 20, 2025
Published: March 1, 2025

antiamyloid, and chemoprotective properties.[16−20] Also, CUR is considered as the most promising natural therapeutic agent against AD. It has been postulated that the prevalence of AD in India is low (4.4 times lower) in comparison with United States due to a higher consumption of CUR.[21] Previous studies have shown that CUR moderately inhibited the enzymes which are emerging as targets for AD treatment such as β-secretase (BACE-1) and glycogen synthase kinase 3 beta (GSK3β).[22,23] Neuroprotective effect of CUR in the Aβ-induced rat AD model has been already reported.[24] However, the broad pharmacological property of CUR is hindered by poor water solubility as well as bioavailability.[25] To support this notion, CUR is absorbed only slightly by the gastrointestinal tract with a maximum level of 11 ng/mL solubility in plain aqueous buffer at acidic pH 5.0. At pH 7.3 (physiological pH), CUR solubility (0.4 μg/mL) was found to be insignificant for its biological activity, as well as the solubilized CUR was found to be sensitive to degradation.[26,27] Low bioavailability of CUR is demonstrated in rats, mice, and humans (that is only 50 ng/mL of CUR has been detected in serum after oral administration of 10 or 12 g/mL).[28] Such a low concentration would have negligible therapeutic effect.[28−30] Hence, to increase the pharmacokinetic properties as well as bioavailability of CUR, numerous strategies have been employed including nanoformulations[31] and synthesizing structural analogues of CUR using amino acids as well as peptides.[32,33] The modification of the phenolic hydroxyl (OH) group of CUR has a great influence on its improved biological functions such as antibacterial and antiproliferative properties.[34]

Indole-3-propionic acid (IPA) is a gut-bacteria-derived metabolite which is widely reported for neuroprotection under various stress conditions such as Aβ-induced neuronal injury,[35] hydroxyl radical-mediated brain injury,[36] ischemia-induced oxidative stress in hippocampus,[37] and neuroinflammation.[38] Keeping these views, in the present study, a diester of CUR with IPA called CUR-IPA was prepared. The in vitro antioxidant activity of CUR-IPA was determined. Further inhibition of CUR-IPA against *Electrophorus electricus* AChE (eAChE), human AChE (hAChE), and human BChE (hBChE) has been determined. In silico docking study was carried out to understand the interaction of CUR-IPA with hAChE and BChE. Molecular dynamics (MD) simulation was performed to determine the stability of the complexes during 200 ns of simulations. Molecular mechanics and generalized Born model and solvent accessibility (MM/GBSA) method was used to calculate the binding energies of the complexes. Principal component analysis (PCA) and dynamic cross-correlation matrix (DCCM) analysis were performed to reveal the dynamic structural alteration in the protein/ligand complexes. Also, quantum mechanics/molecular mechanics (QM/MM) analysis of the protein−ligand was carried out further to understand the interactions.

2. MATERIALS AND METHODS

2.1. Materials. CUR, IPA, eAChE, 2,2′-azino-bis (3-ethylbenzothiazoline-6-sulfonic acid) (ABTS), 1,1-diphenyl-2-picrylhydrazyl (DPPH), 2,4,6-tripyridyl-s-triazine (TPTZ), acetylthiocholine iodide (ATCI), and butyrylthiocholine iodide (BTCI) were purchased from Sigma Chemical Company, USA. All other chemicals were of highest purity and locally purchased.

2.2. Synthesis of CUR-IPA. The reaction mixture consisted of CUR (40 μmol), IPA (550 μmol), dicyclohexylcarbodiimide (200 mg), and 4-dimethylaminopyridine (DMAP; 2 mg) in 15 mL of dichloromethane. The reaction mixture was stirred at room temperature for 12 h. The dicyclohexylurea formed was filtered off. DMAP from the reaction mixture was removed by washing with 5% citric acid. Silica gel (60−120 mesh) column chromatography was done using hexane:ethyl acetate (9:1 to 6:4) to obtain the pure product.

2.3. Characterization of CUR-IPA. CUR and CUR-IPA were solubilized in acetonitrile, and the UV−visible spectra were obtained at room temperature using a UV−visible multi well plate reader (Epoch2, BioTek, USA) by scanning in the wavelength ranging from 200 to 500 nm. Proton and carbon-13 nuclear magnetic resonance (NMR) spectra were obtained with a Bruker spectrophotometer model ultrashield at 400 MHz in DMSO-d6. A Waters Q-Tof micro mass spectrometer was used to obtain the electron spray ionization-mass spectrum (ESI-MS) of CUR-IPA. The purity of CUR-IPA was determined using high-performance liquid chromatography (HPLC) using water and methanol as the solvent (LC-2030C Shimadzu Corporation, Japan).

2.4. In Vitro Antioxidant Activity. The scavenging activity of the radicals by CUR-IPA at various concentrations (200−1000 μM for DPPH radicals and 100−500 μM for ABTS) were determined as described earlier.[39] FRAP activity of CUR-SAC was determined at various concentrations (50−250 μM) using ferric chloride and TPTZ.[40]

2.5. AChE and BChE Enzyme Activity. eAChE purchased from Sigma was used without further purification. Detergent-soluble hAChE was prepared using erythrocyte ghost (membrane) from the human blood sample as described earlier using the homogenization buffer [0.2%, triton X-100 prepared in 50 mM potassium phosphate (KPO_4) buffer, pH 7.4].[39] The serum separated from healthy human blood was used as a source of hBChE. eAChE, hAChE, and hBChE activities were determined as described earlier.[39,41] The reaction mixture (1000 μL) consisted of KPO_4 buffer (100 mM) containing 0.1% bovine serum albumin (pH 7.0), DTNB (2 mM), substrate (1 mM ATCI for eAChE and hAChE or 3 mM BTCI for hBChE), and an aliquot of enzyme. The whole reaction mixture was incubated at 37 °C for 10 min for eAChE as well as hAChE and 5 min for hBChE. The reaction was terminated by the addition of 500 μL of ethanol. The yellow color formed was measured at 412 nm using UV−visible spectroscopy.

2.6. Enzyme Inhibition and Kinetic Analysis. For the enzyme inhibition assay, the enzyme solution in buffer was incubated with different concentrations (2−10 μM for eAChE; 20−100 μM for hAChE and hBChE) of CUR-IPA at room temperature for 30 min. After incubation, the AChE or BChE enzyme activities were determined as given above.

The kinetics of eAChE, hAChE, or hBChE inhibition by CUR-IPA was determined using Lineweaver and Burk double reciprocal plot and Dixon plot.[42,43] For kinetic determination, the concentrations of CUR-IPA used for eAChE and hAChE are 0−10 and 0−100 μM, respectively. ATCI was used in the range of concentrations (0.6−1 mM) in the absence and in the presence of CUR-IPA. Various concentrations of BTCI (1.8−3 mM) were used for hBChE inhibition kinetics in the absence and in the presence of CUR-IPA (0−100 μM).

2.7. Molecular docking, QM/MM, and MD Analysis. The structure of CUR-IPA was drawn using ChemDraw software. The crystal structures of hAChE (PDB ID: 4EY6)

https://doi.org/10.1021/acsomega.4c08149
ACS Omega 2025, 10, 9073−9087

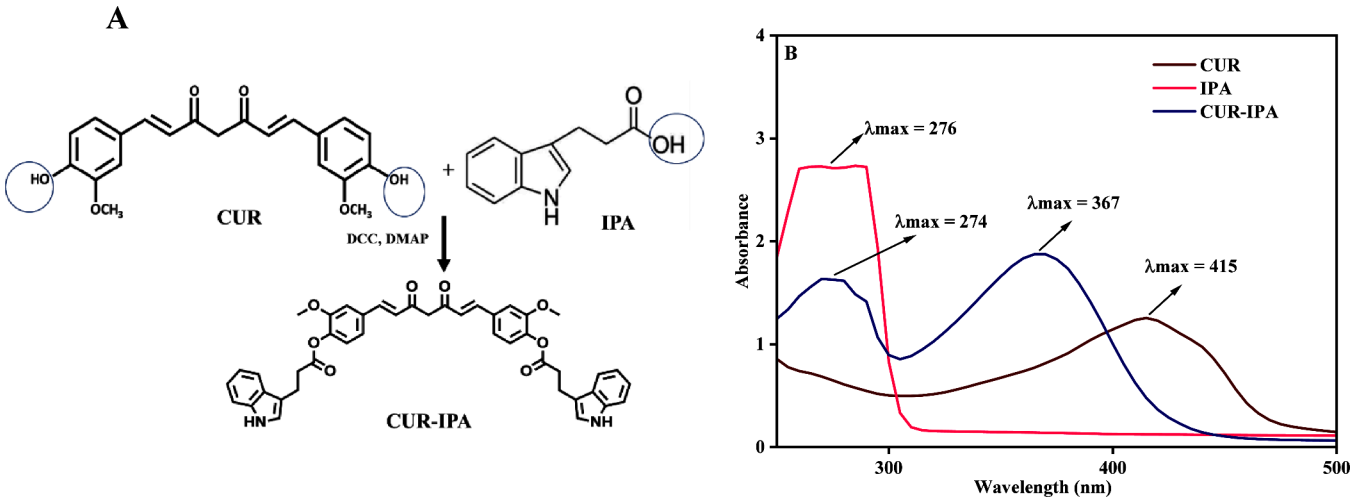

Figure 1. (A) Schematics of CUR-IPA synthesis. (B) UV−visible spectrum of CUR, IPA and CUR-IPA.

and hBChE (PDB ID: 1P0I) were retrieved from the protein data bank.[44,45] The ligands underwent preparation using the Ligprep module within Maestro by Schrödinger. This process involved generating 3D coordinates for all ligands through default ionization and tautomerization. Stereoisomers of the ligands were then produced and optimized by utilizing the OPLS force field. As for the proteins, they were prepared using the protein preparation wizard in Maestro by Schrödinger. This preparation included hydrogen bond optimization and energy minimization of the hydrogen atoms. Following preparation, the proteins and ligands were subjected to docking using the induced fit docking technique employing the extra-precision method. This procedure utilized Maestro and Schrödinger suites Version 2020.1. To facilitate docking, a grid box measuring 10 Å in each dimension was constructed to encompass the binding sites of the target proteins, taking into account the amino acid residues constituting the catalytic and substrate binding sites.

QM is one of the pioneer methods to obtain the electronic level properties of the molecules. The macromolecules like proteins/enzymes and DNA are large in size and also contain more than a thousand atoms in a molecule. Hence, to obtain accurate electronic level information, treating these macromolecules quantum mechanically is quite important. However, it is very difficult to solve the Schrodinger's equation for the large system. Therefore, the QM/MM analysis of protein has been interrogated into two different approaches; one is the major QM region where the ligand interacts with the proximal active site amino acids of the protein. Relatively, the QM region of CUR-IPA/hAChE includes Tyr69, Gly119, Ser122, Glu199, Glu289, Phe292, His444, and CUR-IPA; CUR-IPA/hBChE includes Asn65, Glu194, Gly280, Asn286, Tyr329, His435, and CUR-IPA. The remaining amino acids present in both complexes were treated as the MM region. Therefore, the number of atoms present in the QM region is treated by the Schrodinger equation in the semiempirical PM3 theory implemented in the AmberTools23 package. The remaining part of the protein is considered as the MM region, which excludes the QM region, and this MM region could be treated with Amber force field (all bonded and nonbonded interactions). In addition, few atoms are mimicked as both QM and MM regions, which link between QM and MM regions. The QM/MM energy minimization was carried out with the maximum number of minimization cycles (2000 steps - first 500 steps by the steepest descent method and the remaining steps are systematically carried on the conjugate gradient method), and then it maintained at the micro-canonical ensemble.[46−48] Further, single-point energy calculation has been carried out for CUR, IPA, CUR-IPA in the gas phase, and CUR-IPA/hAChE and CUR-IPA/hBChE using Gaussian09 software with the PM3 basis set.[49] This QM/MM calculation pertains to analyze the intermolecular interactions, HOMO, LUMO, and the corresponding global descriptor properties[50] of CUR-IPA in the gas phase and with respect to the neighboring active site amino acid residues of hAChE and hBChE enzymes.

MD simulation was performed using the OPLS4 force field implemented in the Desmond package. The periodic precondition with 10 $Å^3$ orthorhombic boxes was built. TIP3P water association system was used as the buffer system, and the charged ions (Na^+/Cl^-) were placed isotopically. The MD simulation was carried out up to 200 ns in 2 fs time step with isothermal−isobaric ensemble (NPT), constant temperature (310 K), and pressure (1 bar). MD simulation was performed in triplicate to ensure reproducibility. The parameters such as root-mean-square deviation (RMSD) and root-mean-square fluctuation (RMSF) of CUR-IPA/hAChE and CUR-IPA/hBChE complexes were monitored. The fractions of every 20 ns were used to determine the binding free energy (MM/GBSA) of the protein−ligand complexes by the Prime application available in Schrodinger software package. The PCA and DCCM plots were created with the CPPTRAJ and R-package software.[51,52] The free-energy landscape (FEL) values were obtained using CPPTRAJ and plotted using RinearnGraph3D 5.6 software [https://www.rinearn.com/en-us/].

3. RESULTS

3.1. Characterization of CUR-IPA. The synthesis scheme of CUR-IPA is given in Figure 1A. The UV−vis spectra of CUR, IPA, and CUR-IPA solubilized in acetonitrile are shown in Figure 1B. The λ_{max} for CUR and IPA were found to be 415 and 276 nm, respectively. The λ_{max} for synthesized CUR-IPA was found to be 367 and 274 nm. ^{1}H NMR spectra of CUR exhibited signals for OCH_3, bridged-CH_2, and OH protons at 3.3−3.8, 6−7.3, and 7.52−7.56 ppm, respectively (Figure

https://doi.org/10.1021/acsomega.4c08149
ACS Omega 2025, 10, 9073−9087

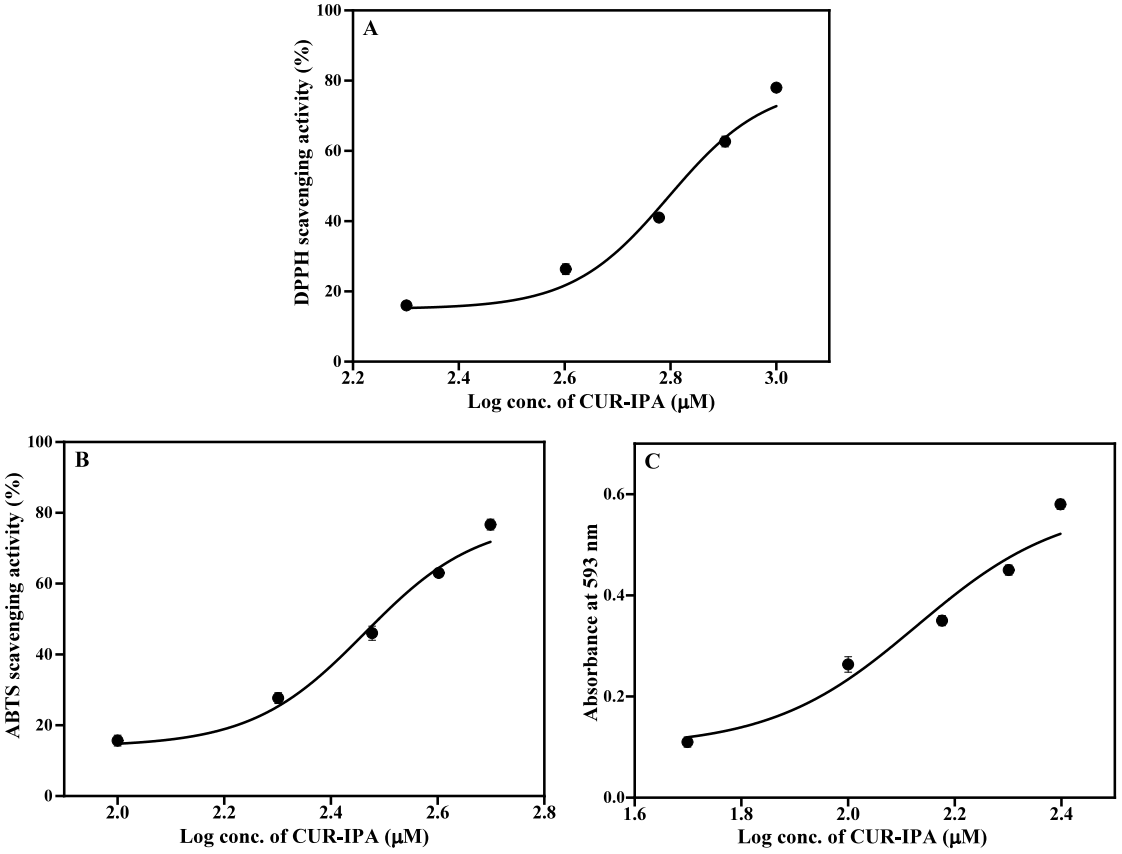

Figure 2. In vitroantioxidant activity of CUR-IPA. (A) DPPH radical scavenging activity. (B) ABTS radical scavenging activity. (C) FRAP activity. $n = 3$.

S1A). IPA exhibited signals for CH_2, indole ring CH, and NH at 2.6−3.4, 6.9−7.5, and 10.78 ppm, respectively (Figure S1B). CUR-IPA showed signals for the protons present in both CUR and IPA, in particular, the presence of NH signals shows the formation of CUR-IPA (Figure S1C). The ^{1}H NMR spectrum of the compound showed a methane (−CH) peak as doublets at 5.88 ppm, related by a ^{13}C NMR spectrum at 33.79 ppm. A singlet peak at 3.32 ppm indicates methoxy proton, related by a ^{13}C NMR spectrum assignable to ($-OCH_3$) methoxy at 56.41 ppm (Figure S1D). HPLC analysis revealed a 97% purity of CUR-IPA (Figure S2). The ESI mass spectrum of CUR-IPA showed a characteristic peak at m/z = 711 (M + H) (Figure S3).

3.2. In Vitro Antioxidant Activity of CUR-IPA. The DPPH and ABTS radical scavenging activities of CUR-IPA are shown in Figure 2A,B. CUR-IPA showed dose-dependent scavenging activity with IC_{50} values of 625.93 and 290.42 μM for DPPH and ABTS, respectively. The FRAP activity of CUR-IPA is shown in Figure 2C. FRAP activity of CUR-IPA increased linearly from 50 to 250 μM concentrations. The IC_{50} values of standard and ascorbic acid for DPPH and ABTS scavenging activities were found to be 34.47 and 15.82 μM (Figure S4A,B). FRAP activity was present linearly in the range from 2 to 10 μM concentrations of ascorbic acid (Figure S4C).

3.3. Inhibition of AChE and BChE by CUR-IPA. eAChE, hAChE, and hBChE were inhibited by CUR-IPA in a dose-dependent manner. The half-maximal inhibitory concentration (IC_{50}) of CUR-IPA against eAChE, hAChE, and hBChE was found to be 5.66, 59.30, and 60.66 μM, respectively (Figure 3A−C). The IC_{50} of standard drugs donepezil and rivastigmine against eAChE and hBChE was 6.4 and 265.51 nm, respectively (Figure S5A,B). The LB plot showing type of inhibition by CUR-IPA against eAChE, hAChE, and hBChE is given in Figure 4A−C, respectively. CUR-IPA showed mixed-type of inhibition against eAChE and hAChE. However, CUR-IPA inhibited hBChE in a competitive manner. Dixon plots revealed the ki value of CUR-IPA against eAChE, hAChE, and hBChE to be 3, 47.14, and 48.99 μM, respectively (Figure 4D−F).

3.4. In Silico Analysis of CUR-IPA with hAChE and hBChE. *3.4.1. Intermolecular Interactions of CUR-IPA-hAChE and hBChE Complexes during Molecular Docking, QM/MM, and MD Simulation.* The docking scores of CUR-IPA with hAChE and hBChE were found to be −16 and −11.41 kcal mol^{-1}. The docking score of donepezil with hAChE and rivastigmine with hBChE was −10.57 and −4.57 kcal mol^{-1}. The superimposed pose of CUR-IPA and donepezil with hAChE as well as CUR-IPA and rivastigmine with hBChE is given in Figure S6. The figure shows that both CUR-IPA and standard drugs are bound in the active sites of the enzymes. Figure 5A,B, respectively, shows the intermolecular interactions of CUR-IPA with hAChE and hBChE enzyme complexes after molecular docking. The comprehensive electronic structure analysis enabled by QM/MM offers profound insights into the interaction between drugs and proteins. This approach delves into intricate binding mechanisms, uncovering subtle phenomena such as hydrogen bonding and charge transfer, which are frequently missed in conventional docking studies. Furthermore, QM/MM's consideration of molecular flexibility offers a dynamic

https://doi.org/10.1021/acsomega.4c08149
ACS Omega 2025, 10, 9073−9087

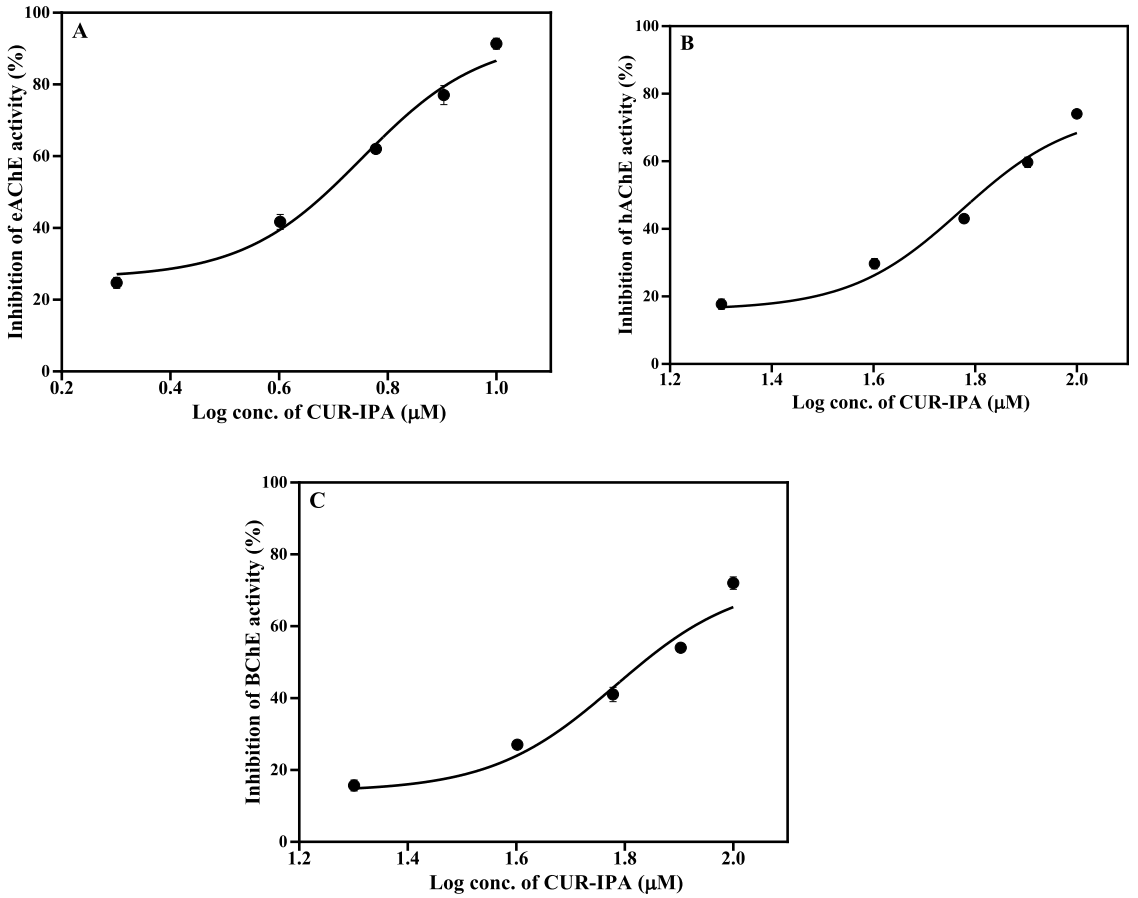

Figure 3. Inhibition of enzyme activity by CUR-IPA. (A) eAChE. (B) hAChE. (C) hBChE. Dose-dependent inhibition of enzyme activity was observed. $n = 3$.

perspective on drug−protein interactions, crucial for elucidating complex binding pathways and mechanisms. Hence, QM/MM minimization of CUR-IPA/hAChE and CUR-IPA/hBChE complexes was carried out. The interaction of CUR-IPA with hAChE and hBChE after QM/MM minimization is shown in Figure 5C,D, respectively. The corresponding neighboring contact distances are listed in Table 1. In docking, CUR-IPA oriented in the active site gorge of hAChE forming interactions with amino acids present in various subsites such as catalytic site (Glu202 and His447), oxyanion hole (Gly120 and Glu121), choline binding site (Trp86), acyl pocket (Phe295), and peripheral anionic site (PAS; Tyr72, Asp74, Tyr124, Trp286, and Tyr341) (Figure 5A and Table 1). CUR-IPA formed hydrophobic interactions with amino acids Tyr72, Leu76, Ala204, Trp236, Trp286, His287, Phe297, Tyr341, and His447. In concordance with hAChE, CUR-IPA oriented in the active site gorge of the hBChE forming hydrogen-bonding interactions with amino acids present in the catalytic site (Ser198 and His438), anionic pocket (Trp82 and Tyr128), and PAS (Asn68 and Tyr332) (Figure 5B and Table 1). Hydrogen bonding was also formed with other amino acids lining the active site gorge such as Thr120, Glu197, Gly283, Thr284, Pro285, and Asn289. Hydrophobic interactions were formed with amino acids, Trp82, Ala227, Pro285, and His438. The intermolecular contacts obtained from molecular docking and QM/MM studies are similar; however, the distance gets varied (Figure 5C,D).

At the end of 200 ns MD simulation, CUR-IPA oriented stably in the active site of hAChE and hBChE forming stable interaction with amino acids similar to that of docking (Figure 6A,B and Table 1). CUR-IPA formed hydrogen bonding with amino acids present in hAChE such as Gln71, Trp86, Tyr124, Ala127, Tyr133, Leu289, Gln291, Glu292, Ser293, Phe295, and Tyr337. CUR-IPA interacted with Leu76, Leu130, Trp286, Phe295, Phe297, and Tyr337 through hydrophobic bonding. In hBChE, CUR-IPA formed a hydrogen bond with Met81, Gly115, Gly116, Gly117, Tyr128, Gly283, Thr284, Pro285, Ser287, Asn289, Ala328, Tyr332, Gly333, Glu352, and His438. Hydrophobic interactions were formed with the amino acids, Phe73, Pro74, Met81, Trp82, Gly283, Thr284, Pro285, Ala328, Phe329, Tyr332, and Pro335 (Figure 6B and Table 1). To better understand the interaction of CUR-IPA with hAChE and hBChE throughout simulation, the interaction figures at every 50 ns are shown in Figures S7 and S8, respectively. Further, the percentage and type of interactions with amino acids present in the active site gorge of hAChE and hBChE are shown in Figure S9. In the case of hAChE, the orientation of CUR-IPA was stabilized within 50 ns of MD simulation. After 50 ns, only meager changes in the interaction of CUR-IPA with amino acids of hAChE could be observed. In the simulation interaction diagram, it is clear that CUR-IPA formed a hydrogen bond with amino acids Tyr133, Phe295, and Arg296 and hydrophobic interactions with Gly82 and Trp286 for a high percentage of time (Figure S7). In hBChE, similar to hAChE, the orientation of CUR-IPA in the active site gorge stabilized after 50 ns of MD simulation, which was almost similar at the end of 200 ns simulation (Figure S8). In particular, the interaction with catalytic amino acid, His438,

https://doi.org/10.1021/acsomega.4c08149
ACS Omega 2025, 10, 9073−9087

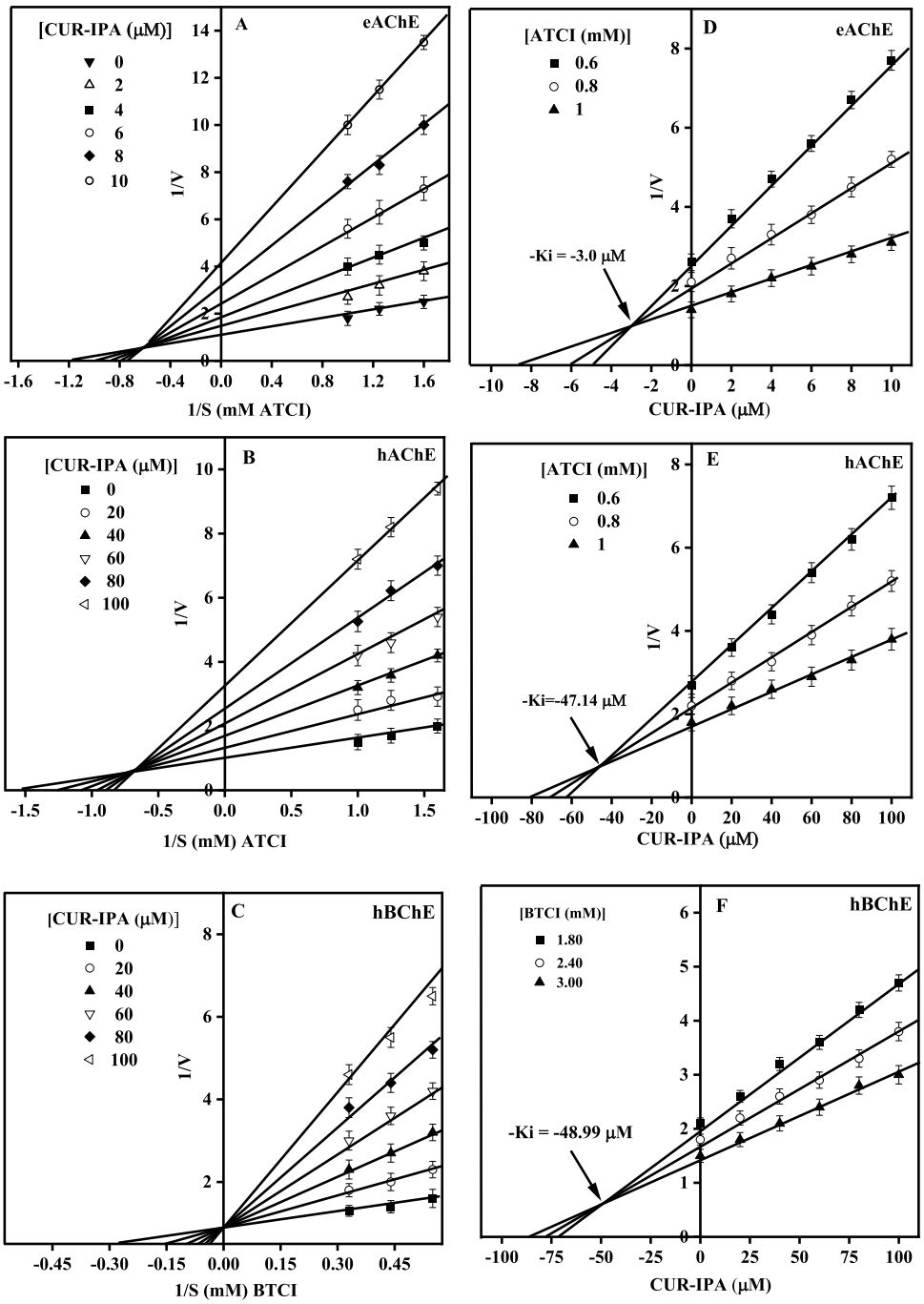

Figure 4. Kinetics of enzyme inhibition by CUR-IPA. LB plot of CUR-IPA against (A) eAChE, (B) hAChE, and (C) hBChE showing the type of inhibition. Dixon plot of CUR-IPA against (D) eAChE, (E) hAChE, and (F) hBChE showing the inhibitor constant.

although lost at the beginning of MD simulation, was reestablished and found to be present even at the end of 200 ns MD simulation. This shows that CUR-IPA is stably placed in the active site of hBChE.

3.4.2. Drug-likeness Properties and Global Descriptor Values of CUR-IPA. The drug-likeness properties of CUR-IPA are given in Table S1. The HOMO and LUMO plots in the gas phase and active site of hAChE and hBChE are shown in Figure 7. The blue and red colors represent the positive and negative phases of the molecules. The global reactivity descriptors such as the band gap energy, ionization potential, electron affinity, global hardness, electronic chemical potential, electrophilicity, and electronegativity index are listed in Table 2.

3.4.3. RMSD, RMSF, and MM/GBSA Analysis of CUR-IPA-hAChE and hBChE Complexes. The RMSD of hAChE/CUR-IPA and hBChE/CUR-IPA complexes throughout 200 ns MD simulations are shown in Figure 8A,B. The difference in RMSD was found to be less than 1.0 Å, which indicates the stable binding of CUR-IPA with the proteins. RMSF value showed that fluctuations were prominent in the N and C-terminals of hAChE/CUR-IPA and hBChE/CUR-IPA complexes during MD simulation (Figure 8C,D). Also, fluctuations of amino acids present in the PAS and anionic pocket amino acids of these proteins are observed. The RMSD (Figure S10A,B) and

https://doi.org/10.1021/acsomega.4c08149
ACS Omega 2025, 10, 9073−9087

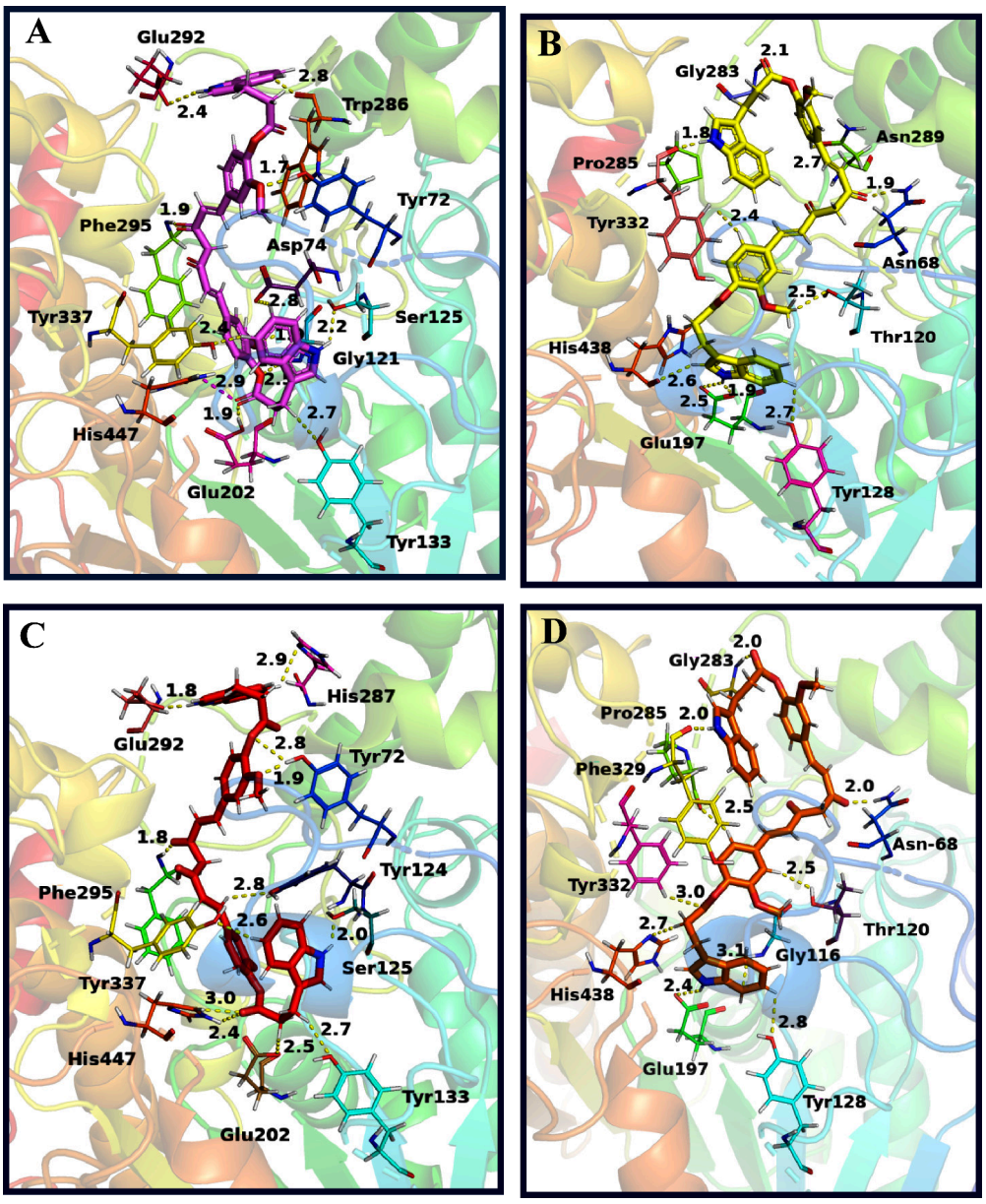

Figure 5. Interaction of CUR-IPA with proteins. (A) Docked pose of hAChE/CUR-IPA. (B) Docked pose of hBChE/CUR-IPA, (C) hAChE/CUR-IPA at the end of QM/MM, and (D) hBChE/CUR-IPA at the end of QM/MM.

RMSF (Figure S10C,D) of MD triplicates are given in the figure. There was no alteration in the RMSD and RMSF values between the replicates, which indicates the reproducibility of the results. The changes in the binding free energy, electrostatic interactions (Coulomb) energy, lipophilic interaction (Lipo) energy, and van der Waals (VdW) energy throughout the 200 ns MD simulation of CUR-IPA/hAChE and CUR-IPA/hBChE are shown in Figure 9A,B, respectively. All of these various energies contributed to the formation of stable binding between CUR-IPA and proteins (hAChE and hBChE).

3.4.4. PCA, DCCM, and FEL Analysis of CUR-IPA-hAChE and hBChE Complexes. The PCA plots of CUR-IPA/hAChE and CUR-IPA/hBChE enzyme complexes are shown in Figure 10A,B. The eigen values of the complexes were plotted against the eigen vector index. The dominant movements of the complexes are related to the first five eigenvectors and the higher eigenvalue. Followed by that, the complex showed no considerable variations in the calculated eigen fraction following 5 until 20 eigen values and reached the static elbow point. The PC1 values of the CUR-IPA/hAChE and CUR-IPA/hBChE enzyme complex are 20.47 and 37.73%, respectively. High PC1 values denote the large motion of the complex system, and it is related to the lower stability of the complex. Hence the CUR-IPA/hAChE complex undergoes lower motion than the latter and denotes the high stability of the same. The FEL in accordance with the PC values of Cα atoms during MD simulation is an ideal technique for conformational sampling. The complex correlation of the atomic motion of the system is used to determine the functional motion of the macromolecules. Hence, the conformation space of CUR-IPA/hAChE and CUR-IPA/hBChE complexes in accordance with the energy and time has been plotted as the FEL surface, and it is shown in Figure 10C,D. The minimum energy conformation occurs at the time period of 29 and 67 ns for CUR-IPA/hAChE and CUR-IPA/

https://doi.org/10.1021/acsomega.4c08149
ACS Omega 2025, 10, 9073−9087

Table 1. Details of the CUR-IPA Interaction with Various Amino Acids Present in AChE and BChE at the End of Docking and 200 ns MD Simulation

protein–ligand complex	docking/MD	interacting amino acid residues (distance Å)	
		hydrogen bond	hydrophobic interaction
hAChE-CUR-IPA	docking	Tyr72 (1.7), Asp74 (2.8), Trp86 (4.2), Gly120 (2.6), Gly121 (2.2, 2.5), Gly122 (1.9), Tyr124 (3.3), Ser125 (2.2), Tyr133 (2.7), Glu202 (1.9), Trp286 (3.6), Glu292 (2.4), Phe295 (1.9), Tyr337 (2.4), Tyr341 (3.3), His447 (3.1)	Tyr72 (4.9), Leu76 (4.5), Ala204 (4.0), Trp236 (4.6), Trp286 (4.4), His287 (5.2), Phe297 (4.7), Tyr341 (5.2), His447 (4.6)
	QM/MM	Tyr72 (1.9), Gly120 (2.1), Gly121 (2.1), Tyr124 (2.8), Ser125 (2.0), Tyr133 (2.7), Glu202 (2.5), Ala204 (2.5), His287 (2.9), Glu292 (1.8), Phe295 (1.8), Tyr337 (2.1), His447 (2.4)	Tyr72 (5.1), Trp86 (4.5), Ala204 (4.5), Phe297 (4.9), Tyr341 (5.3)
	MD	Gln71 (3.5), Trp86 (3.0), Tyr124 (2.6), Ala127 (2.9), Tyr133 (2.0), Leu289 (2.3), Gln291 (2.4), Glu292 (3.3), Ser293 (2.6), Phe295 (2.7), Tyr337 (2.1)	Leu76 (5.3), Leu130 (5.1), Trp286 (5.8), Phe295 (4.8), Phe297 (5.4), Tyr337 (4.5)
hBChE-CUR-IPA	docking	Asn68 (1.9), Trp82 (3.4), Thr120 (2.5), Tyr128 (2.7), Glu197 (1.9, 2.5), Ser198 (3.6), Gly283 (2.1), Thr284 (3.3), Pro285 (2.4), Asn289 (2.7), Tyr332 (1.8), His438 (2.6)	Trp82 (4.2), Ala227 (4.3), Pro285 (4.3), His438 (5.2)
	QM/MM	Asn68 (2.0), Gly116 (3.1), Thr120 (2.9), Tyr128 (2.8), Glu197 (2.4), Val280 (2.0), Gly283 (2.8), Pro285 (2.0), Phe325 (2.5), Tyr332 (2.0), His437 (2.8)	Trp79 (4.4), Ala274 (4.3), Pro282 (4.3)
	MD	Met81 (3.7), Gly115 (3.2), Gly116 (2.8), Gly117 (3.4), Tyr128 (2.8), Gly283 (3.5), Thr284 (2.8), Pro285 (3.7), Ser287 (3.7), Asn289 (2.0), Ala328 (3.0), Tyr332 (2.4), Gly333 (3.3), Glu352 (3.1), His438 (3.2)	Phe73 (5.3), Pro74 (5.2), Met81 (4.8), Trp82 (5.3), Gly283 (4.1), Thr284 (4.1), Pro285 (5.1), Ala328 (4.4), Phe329 (4.2), Tyr332 (5.0), Pro335 (4.8)

hBChE complexes, respectively. The pair-wise cross-correlation calculation is one of the pioneer techniques to find the pair-wise alignment of residues with respect to the ligand in the complex system. Figure 11A,B shows the DCCM plots of the CUR-IPA/hAChE and CUR-IPA/hBChE enzymes. Similar to PCA, in DCCM, CUR-IPA/hBChE correlated motions were found to be high in comparison to CUR-IPA/hAChE. In both complexes, the anticorrelated motion was found to be less throughout MD simulation. Altogether, CUR-IPA/hAChE was found to be dynamically stable in comparison to the CUR-IPA/hBChE complex.

4. DISCUSSION

CUR-IPA diester was synthesized and characterized. CUR-IPA showed in vitro antioxidant and ChEs showed inhibitory activity. Further CUR-IPA interacted with the amino acids present in the active site gorge of hAChE and hBChE. CUR is known for numerous neuroprotective properties such as antioxidant effect,[53] inhibition of Aβ fibril formation,[54] destabilization of formed Aβ fibril,[20] increase of the endogenous antioxidant level through activation of nuclear factor erythroid 2-related factor 2,[55] and anti-inflammatory effect through inhibition of nuclear factor kappa B (NF-κB).[56] However, bioavailability of CUR is very low, and hence various analogues of CUR are synthesized.[57] Glucuronidation and sulfation of phenolic OH group of CUR lead to its metabolism and excretion.[58] In previous studies, the OH group was esterified with glycine, glutamic acid, valine, demethylenated piperic acid, and piperic acid-glycine.[34,59,60] The dipiperoyl and diglycinoyl derivatives showed higher apoptotic activity against cancer cell lines.[60] In another study, conjugates of CUR with amino acids, alanine, valine, serine, and cysteine, improved the water solubility of CUR and its antimutagenic activity.[61] CUR-glutamic acid diesters were reported for improved protection in comparison to CUR against glutathione depletion-mediated oxidative stress in neuronal cells.[62] Monoester and diester of CUR-lysine have shown inhibition effect on lysozyme amyloid fibrillation.[33] Other than CUR-amino acid conjugates, sugar-CUR conjugate has been synthesized previously.[63] The sugar-CUR inhibited Aβ and tau peptide aggregation at low concentrations in comparison to CUR.[63] Due to masking of the phenolic OH group of CUR, these conjugates have improved bioavailability through enhanced adsorption and slow metabolism.[34,59,60,62] In concordance with these previous studies, CUR-IPA was synthesized, and the anticholinesterase effect is well documented in the present study. Conjugation of CUR with IPA would be advantageous since IPA is known for various biological activities, in particular, the neuroprotective effect against various stress conditions.[35−38] In addition, IPA is a potent antioxidant through scavenging of free radicals and stabilization of mitochondrial electron transport, thereby inhibiting the radical generation.[35,64] IPA through electron donation neutralizes the highly reactive hydroxyl radicals, and unlike other antioxidants (ascorbic acid and tocopherol), IPA does not generate pro-oxidant intermediates while neutralizing free radicals.[35,64,65] Hence, conjugation of IPA with CUR could be considered advantageous over other compounds. In a previous study, CUR was reported for only low inhibitory activity against eAChE (IC_{50} = 51.8 μM), whereas CUR did not show inhibition against BChE.[66] In the rat cadmium-induced toxicity model, CUR was found to decrease the AChE gene expression and its activity in the cortex. Also, it has been found that CUR inhibited rat cerebral cortex AChE with an

https://doi.org/10.1021/acsomega.4c08149
ACS Omega 2025, 10, 9073−9087

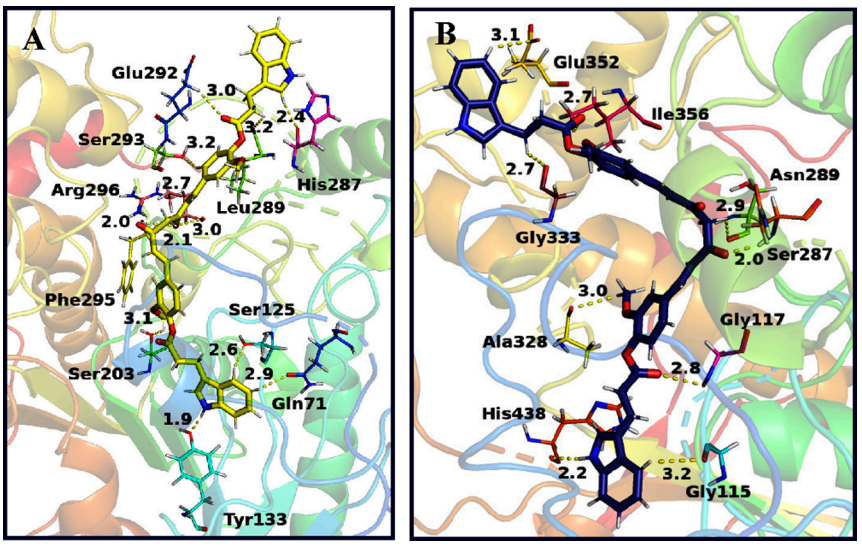

Figure 6. Interaction of CUR-IPA with hAChE (A) and hBChE (B) at the end of the 200 ns MD simulation.

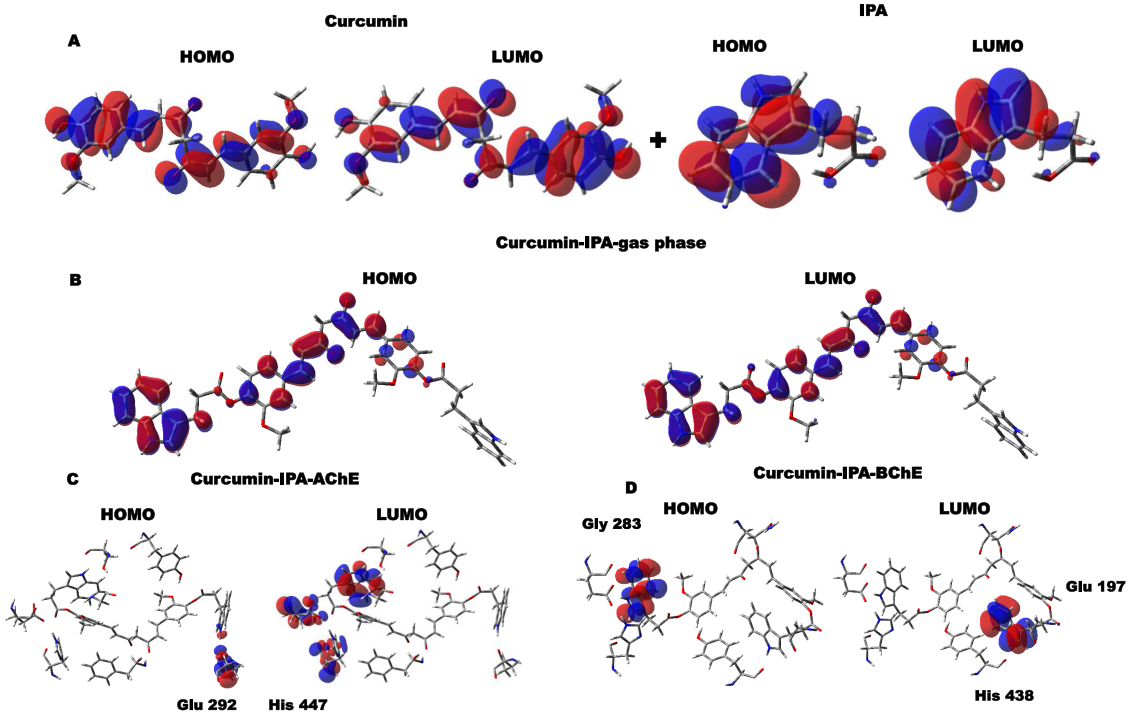

Figure 7. HOMO and LUMO of CUR-IPA in gas phase (A), hAChE (B), and hBChE (C).

Table 2. Globular Descriptors of CUR, IPA, and CUR-IPA in Different Environments

molecular descriptors	CUR	gas phase IPA	CUR-IPA	CUR-IPA hAChE	CUR-IPA hBChE
band gap energy (eV)	0.0955	0.1405	0.0673	0.0689	0.2133
HOMO energy (eV)	−0.3111	−0.3037	−0.2865	−0.2296	−0.3193
LUMO energy (eV)	−0.2156	−0.1632	−0.2192	−0.2985	−0.1060
ionization potential ($I = -E_{HOMO}$)	0.3111	0.3037	0.2865	0.2296	0.3193
electron affinity ($A = -E_{LUMO}$)	0.2156	0.1632	0.2192	0.2985	0.1060
global hardness $\eta = (I - A)/2$	0.0478	0.0702	0.0337	0.0345	−0.1067
electronic chemical potential $\mu = -(I + A)/2$	−0.2634	−0.2335	−0.2529	−0.3789	−0.2127
$\omega = \mu^2/2\eta$	0.7263	0.3881	0.9500	2.0831	0.2120
electronegativity $\chi = (I + A)/2$	0.2634	0.2335	0.2529	0.3789	0.2127

https://doi.org/10.1021/acsomega.4c08149
ACS Omega 2025, 10, 9073−9087

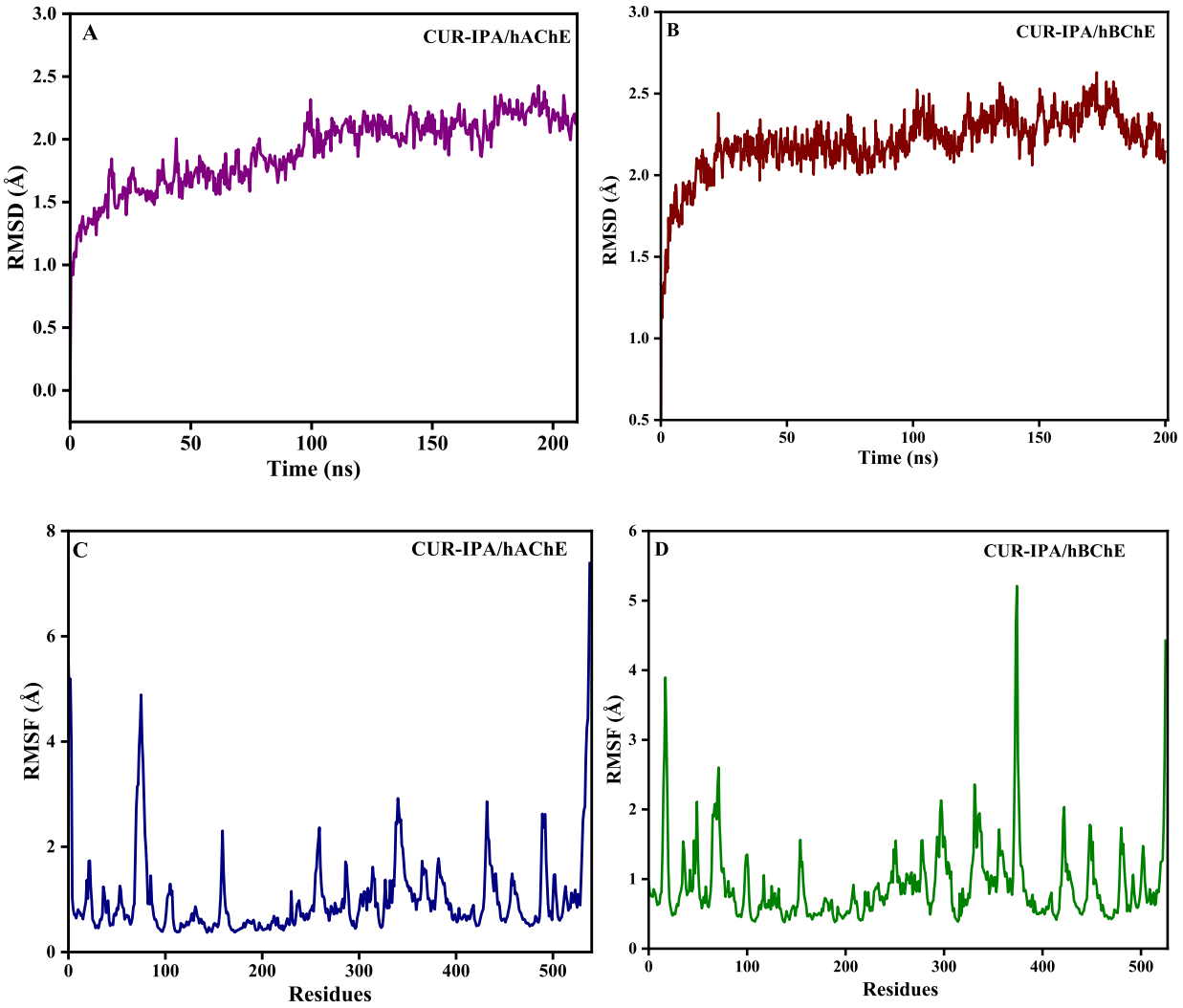

Figure 8. RMSD (A, B) and RMSF (C, D) of hAChE/CUR-IPA and hBChE/CUR-IPA complexes.

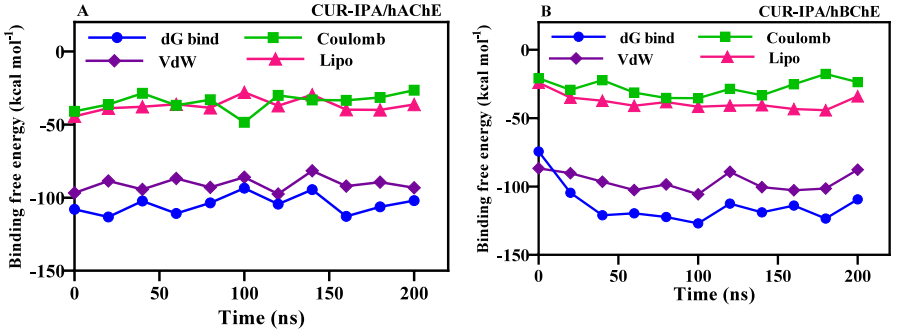

Figure 9. Binding free-energy analysis by MM/GBSA. The plot shows the binding free energy and Coulomb (electrostatic), vdW, and Lipo energy fluctuations as a function of simulation time for the complexes CUR-IPA/hAChE (A) and CUR-IPA/hBChE (B).

IC_{50} value of 10 μM.[67] In another study, CUR inhibited eAChE with an IC_{50} value of 67.69 μM.[68] In the same study, it has been found that CUR did not affect AChE activity in the *ex vivo* model. The explanation for such an effect would be the poor absorption and limited penetration into the brain.[68] IPA showed inhibition against AChE and BChE at concentrations $\geq$ 500 μM (data not shown). However, conjugation of IPA with CUR had improved inhibitory activity against eAChE in the present study with an IC_{50} value of 5.66 μM. Also, CUR-IPA showed inhibition against hAChE and hBChE. Since IPA has good penetration capacity into the brain, it has been increasingly studied for the protective effect against neurological disorders.[69] Hence, the conjugation of IPA with CUR might increase the penetration of CUR-IPA into the brain, which is yet to be determined. AChE-Aβ complex is found to be highly toxic in comparison to Aβ alone.[70] The PAS of AChE is involved in noncholinergic functions of the enzyme such as in the Aβ aggregation.[71−73] Due to these reasons, PAS or dual-site (catalytic and peripheral) inhibitors are emerging as an attractive target for the design of new antidementia drugs. Such

https://doi.org/10.1021/acsomega.4c08149
ACS Omega 2025, 10, 9073−9087

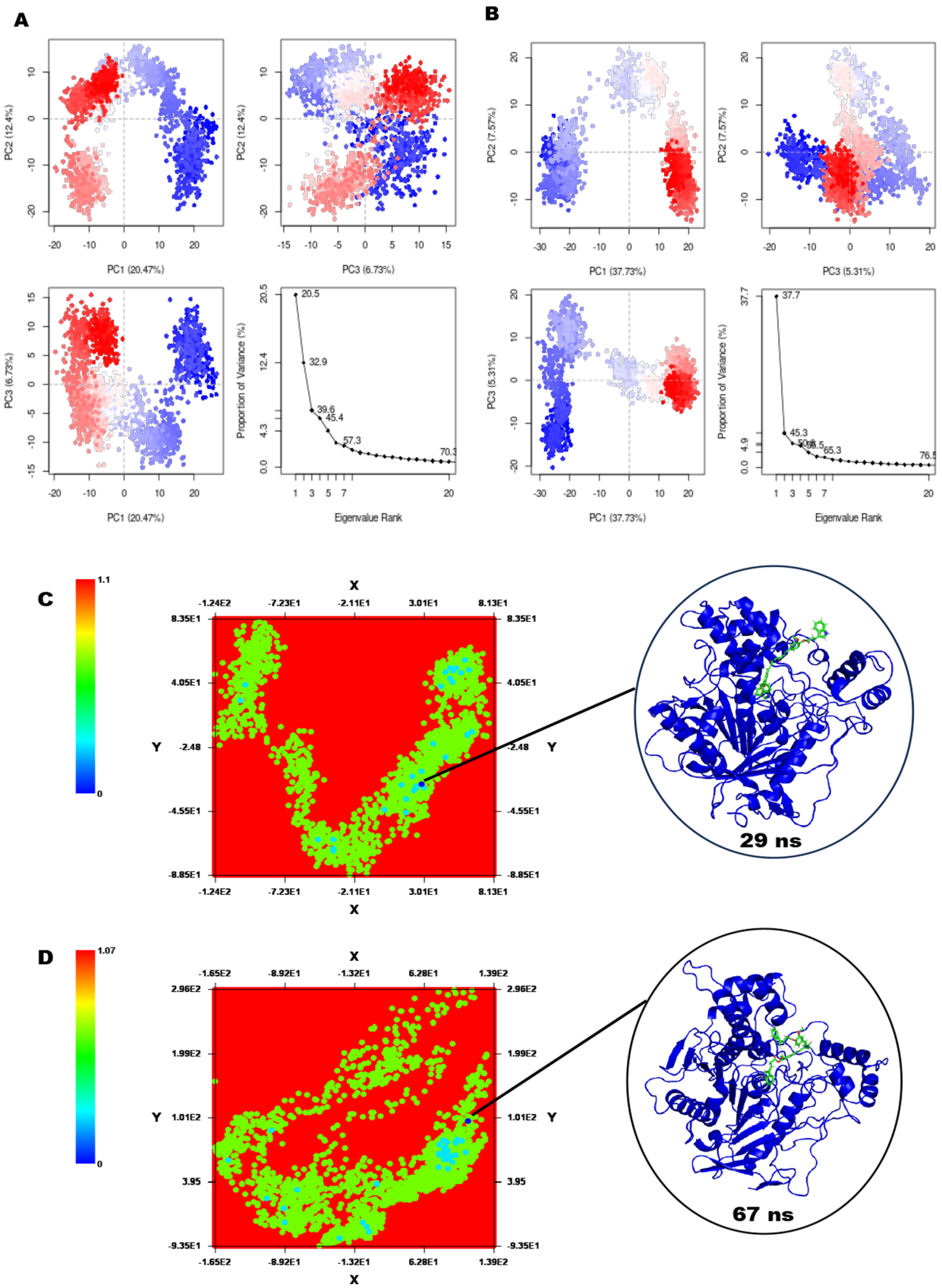

Figure 10. PCA (A, B) and FEL (C, D) plots of hAChE/CUR-IPA and hBChE/CUR-IPA complexes.

drugs might simultaneously alleviate the cognitive deficit in Alzheimer's patients as well as inhibit the assembly of Aβ, thereby reducing neuronal degeneration. In silico analysis clearly indicated the interaction of CUR-IPA with amino acids present in the catalytic site as well as PAS of both AChE and BChE. Further, MD analysis confirmed the stable binding of

https://doi.org/10.1021/acsomega.4c08149
ACS Omega 2025, 10, 9073−9087

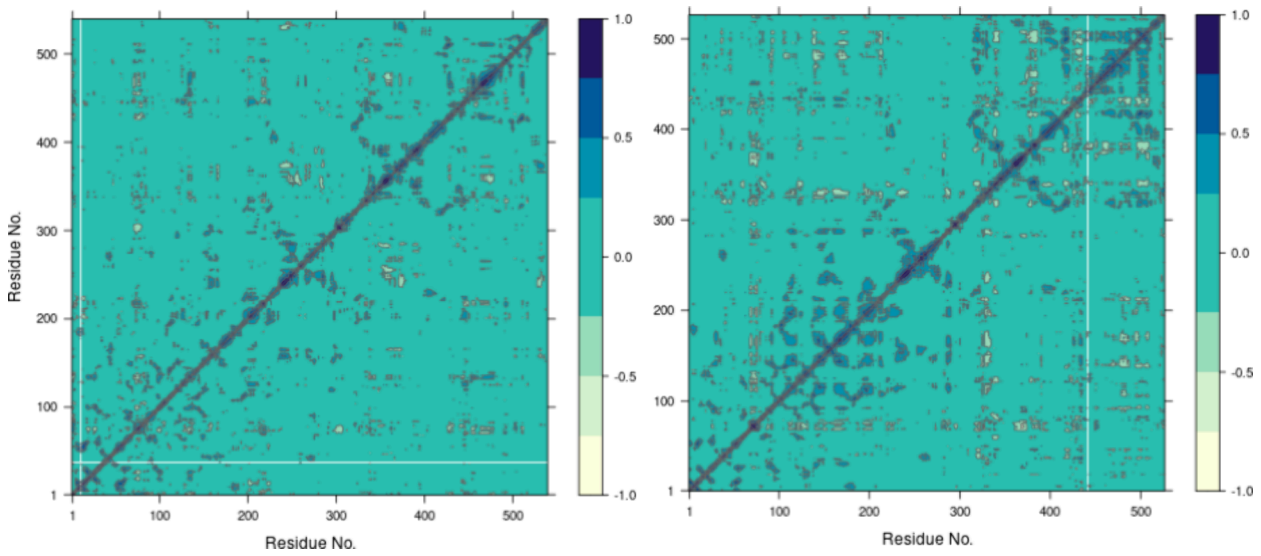

Figure 11. DCCM plots of the hAChE/CUR-IPA (A) and hBChE/CUR-IPA (B) complexes.

CUR-IPA in these enzymes. CUR-IPA interacted with the amino acids present in various subsites such as the catalytic site, oxyanion hole, choline binding site, acyl pocket, and PAS of both AChE and BChE. Among the drugs approved for AD treatment, rivastigmine inhibits both hAChE and hBChE, whereas donepezil and galantamine are selective inhibitors of hAChE.[7,74,75] Since rivastigmine inhibits both hAChE and hBChE, it has been found to benefit executive dysfunction found in subcortical dementias.[75] Donepezil binds to both the catalytic site and PAS of AChE. Such a dual-binding nature of donepezil has given an advantage of inhibition of Aβ aggregation.[71] Galantamine binds to only the catalytic site of hAChE. Hence, galantamine-CUR hybrids were designed to contain galantamine as the core and aromatic moiety of CUR, both linked by the linker. These hybrids showed dual-site binding ability in AChE, that is, galantamine interacted in the active site of hAChE, whereas the aromatic moiety linked to these hybrid molecules interacted with PAS.[76] In comparison to these known inhibitors, CUR-IPA inhibited both hAChE and hBChE as well as interacted with both the catalytic site and PAS. Also, these known drugs, galantamine, rivastigmine, and donepezil, present various side effects; however, CUR and IPA are known for low toxicity as well as multiple neuronal protective functions.[22−24,35−38] Hence, CUR-IPA could be considered advantageous over these known inhibitors of ChEs, which need further validation through cell line and in vivo studies.

The minimum energy state contributes to the reaction phase of the protein complex structure,[77] and FEL analysis helped to find the reaction coordinates of both complexes. Due to presence of various functional groups in CUR-IPA, hydrogen bonding, hydrophobic interaction, and vdW forces have contributed for such stable binding of CUR-IPA. In in silico, the binding of CUR-IPA was found to be similar to that of CUR from previous study.[78] Global reactivity descriptors of CUR-IPA explain the binding nature of the molecule in the active site according to their energy level at the gas phase and the hAChE and hBChE active sites. The band gap energy is the measure of the chemical reactivity of the complex system. According to the band gap energy value, IPA exhibits more chemical reactivity nature than CUR and due to the redistribution of charges, CUR-IPA displays less chemical reactivity, indicating the high stability of the structure. Further, the hAChE/CUR-IPA enzyme complex shows a low reactive rate, which implies that CUR-IPA is stabilized within the active site of the hAChE enzyme, and the probability of the molecule to leave the active site is quite low. Global hardness is the measure of the stability of the system. CUR (0.0478) decreases the rigidness of IPA (0.0702), which leads to more reactivity of CUR-IPA (0.0337). Relatively, in an active site environment, the stability of CUR-IPA with respect to active site amino acids of hBChE is lower. High HOMO energy value of the molecule in the active site of hAChE is due to the HOMO charge redistribution near the interacting region of the negatively charged amino acid Glu292. The high LUMO energy value of hBChE/CUR-IPA is due to the LUMO charge redistribution near residues Glu197 and His438. Electrophilicity is the measure of tendency of the molecule to react with the protein/enzyme.[79] Based on the electrophilicity index and electronegativity values, CUR-IPA was found to be tightly bound with the active site amino acids of hAChE than the hBChE enzyme. In MD analysis (RMSD, MM/GBSA, PCA, and DCCM) and QM/MM analysis, it has been found that hAChE/CUR-IPA complex is highly stable in comparison to hBChE. Global dynamic motion of the hAChE/CUR-IPA complex has been found to be less; thereby, it is inferred that CUR-IPA binding has stabilized the structure of hAChE. Previously, IPA was conjugated with tacrine (a catalytic site inhibitor) using various sizes of alkyl chain linkers to target both the catalytic site and PAS of AChE. These derivatives were patented as inhibitors of AChE (European patent no. EP 1 646 622 B1). In the case of CUR-IPA, the presence of seven carbon linkers in CUR has been advantageous and helped in the orientation of CUR-IPA throughout active site gorge forming interaction with amino acids present in both the catalytic site and PAS of AChE.

5. CONCLUSIONS

Diester of CUR with IPA (CUR-IPA) was synthesized. CUR-IPA showed in vitro antioxidant activity. Further, CUR-IPA inhibited both AChE and BChE in vitro. In silico analysis revealed the stable binding of CUR-IPA in the active site gorge of both AChE and BChE. CUR-IPA interacted with amino

https://doi.org/10.1021/acsomega.4c08149
ACS Omega 2025, 10, 9073−9087

acids present in both the catalytic site and PAS of these enzymes. Post-MD simulation analyses as well as QM/MM analysis indicated that the hAChE/CUR-IPA complex is stable in comparison to hBChE/CUR-IPA. Hence, CUR-IPA could act as a cognitive enhancer under neurodegenerative disease conditions through inhibition of catalytic function of the enzyme as well as hindering Aβ aggregation. Further in vivo study is required to understand the application of CUR-IPA in the treatment of cognitive dysfunction.

■ ASSOCIATED CONTENT

Data Availability Statement

All data are included either as figures or tables within the manuscript.

Supporting Information

The Supporting Information is available free of charge at https://pubs.acs.org/doi/10.1021/acsomega.4c08149.

NMR spectra, HPLC chromatogram, ESI spectra, and drug-likeness properties of the synthesized compound and additional in vitro and in silico results (PDF)

■ AUTHOR INFORMATION

Corresponding Author

Palvannan Thayumanavan − *Department of Biochemistry, Periyar University, Salem, Tamil Nadu 636011, India;* orcid.org/0000-0003-1023-0806; Phone: +91-9894280618; Email: pal2912@periyaruniversity.ac.in

Authors

Jayanthi Sidhambaram − *Department of Biochemistry, Periyar University, Salem, Tamil Nadu 636011, India*

Penislusshiyan Sakayanathan − *Bioinnov Solutions LLP, Research and Development Center, Salem, Tamil Nadu 636009, India*

Chitra Loganathan − *Department of Prosthodontics and Implantology, Saveetha Dental College and Hospital, Saveetha Institute of Medical and Technical Sciences (SIMATS), Chennai 600 077, India*

Ancy Iruthayaraj − *Bioinnov Solutions LLP, Research and Development Center, Salem, Tamil Nadu 636009, India*

Complete contact information is available at: https://pubs.acs.org/10.1021/acsomega.4c08149

Author Contributions

J.S. and P.S. designed the research study and performed the research. C.L. analyzed the data and wrote the paper. A.I. performed computational study. P.T. supervised the research and edited the final draft.

Notes

The authors declare no competing financial interest.

■ ACKNOWLEDGMENTS

Mrs. J.S. acknowledges the Periyar University for the award of University research fellowship (PU/AD-3URF Order/13629/23F81492/2023).

■ REFERENCES

(1) Parihar, M.; Hemnani, T. Alzheimer's disease pathogenesis and therapeutic interventions. *Journal of clinical neuroscience* **2004**, *11* (5), 456−467.

(2) Ballard, C. G.; Greig, N. H.; Guillozet-Bongaarts, A. L.; Enz, A.; Darvesh, S. Cholinesterases: roles in the brain during health and disease. *Current Alzheimer Research* **2005**, *2* (3), 307−318.

(3) Jivad, N.; Rabiei, Z. A review study on medicinal plants used in the treatment of learning and memory impairments. *Asian Pacific Journal of Tropical Biomedicine* **2014**, *4* (10), 780−789.

(4) Liu, Y.; Liu, H.; Yang, J.; Liu, X.; Lu, S.; Wen, T.; Xie, L.; Wang, G. Increased amyloid β-peptide (1−40) level in brain of streptozotocin-induced diabetic rats. *Neuroscience* **2008**, *153* (3), 796−802.

(5) Peila, R.; Rodriguez, B. L.; Launer, L. J. Type 2 diabetes, APOE gene, and the risk for dementia and related pathologies: The Honolulu-Asia Aging Study. *Diabetes* **2002**, *51* (4), 1256−1262.

(6) Hampel, H.; Mesulam, M. M.; Cuello, A. C.; Khachaturian, A. S.; Vergallo, A.; Farlow, M. R.; Snyder, P. J.; Giacobini, E.; Khachaturian, Z. S.; Cholinergic System Working, G.; et al. Revisiting the cholinergic hypothesis in Alzheimer's disease: emerging evidence from translational and clinical research. *J. Prevent. Alzheimer's Dis.* **2019**, *6*, 2−15.

(7) Marucci, G.; Buccioni, M.; Dal Ben, D.; Lambertucci, C.; Volpini, R.; Amenta, F. Efficacy of acetylcholinesterase inhibitors in Alzheimer's disease. *Neuropharmacology* **2021**, *190*, No. 108352.

(8) Inestrosa, N. C.; Alvarez, A.; Perez, C. A.; Moreno, R. D.; Vicente, M.; Linker, C.; Casanueva, O. I.; Soto, C.; Garrido, J. Acetylcholinesterase accelerates assembly of amyloid-β-peptides into Alzheimer's fibrils: possible role of the peripheral site of the enzyme. *Neuron* **1996**, *16* (4), 881−891.

(9) Mushtaq, G.; Greig, N. H.; Khan, J. A.; Kamal, M. A. Status of acetylcholinesterase and butyrylcholinesterase in Alzheimer's disease and type 2 diabetes mellitus. *CNS & Neurological Disorders-Drug Targets (Formerly Current Drug Targets-CNS & Neurological Disorders)* **2014**, *13* (8), 1432−1439.

(10) Darvesh, S.; Cash, M. K.; Reid, G. A.; Martin, E.; Mitnitski, A.; Geula, C. Butyrylcholinesterase is associated with β-amyloid plaques in the transgenic APPSWE/PSEN1dE9 mouse model of Alzheimer disease. *Journal of Neuropathology & Experimental Neurology* **2012**, *71* (1), 2−14.

(11) Ulrich, J.; Meier-Ruge, W.; Probst, A.; Meier, E.; Ipsen, S. Senile plaques: staining for acetylcholinesterase and A4 protein: a comparative study in the hippocampus and entorhinal cortex. *Acta neuropathologica* **1990**, *80*, 624−628.

(12) Misrani, A.; Tabassum, S.; Yang, L. Mitochondrial dysfunction and oxidative stress in Alzheimer's disease. *Frontiers in aging neuroscience* **2021**, *13*, No. 617588.

(13) Butterfield, D. A.; Drake, J.; Pocernich, C.; Castegna, A. Evidence of oxidative damage in Alzheimer's disease brain: central role for amyloid β-peptide. *Trends in molecular medicine* **2001**, *7* (12), 548−554.

(14) Orhan, I.; Aslan, M. Appraisal of scopolamine-induced antiamnesic effect in mice and in vitro antiacetylcholinesterase and antioxidant activities of some traditionally used Lamiaceae plants. *Journal of Ethnopharmacology* **2009**, *122* (2), 327−332.

(15) Mimica, N.; Presečki, P. Side effects of approved antidementives. *Psychiatria Danubina* **2009**, *21* (1), 108−113.

(16) El-Maddawy, Z. K.; El-Sayed, Y. S. Comparative analysis of the protective effects of curcumin and N-acetyl cysteine against paracetamol-induced hepatic, renal, and testicular toxicity in Wistar rats. *Environmental science and pollution research* **2018**, *25*, 3468−3479.

(17) Hewlings, S. J.; Kalman, D. S. Curcumin: A review of its effects on human health. *Foods* **2017**, *6* (10), 92.

(18) Zorofchian Moghadamtousi, S.; Abdul Kadir, H.; Hassandarvish, P.; Tajik, H.; Abubakar, S.; Zandi, K. A review on antibacterial, antiviral, and antifungal activity of curcumin. *BioMed. Res. Int.* **2014**, *2014*, No. 186864.

(19) Gupta, S. C.; Patchva, S.; Koh, W.; Aggarwal, B. B. Discovery of curcumin, a component of golden spice, and its miraculous biological activities. *Clinical and experimental pharmacology and physiology* **2012**, *39* (3), 283−299.

(20) Yang, F.; Lim, G. P.; Begum, A. N.; Ubeda, O. J.; Simmons, M. R.; Ambegaokar, S. S.; Chen, P. P.; Kayed, R.; Glabe, C. G.; Frautschy, S. A. Curcumin inhibits formation of amyloid β oligomers and fibrils, binds plaques, and reduces amyloid in vivo. *J. Biol. Chem.* **2005**, *280* (7), 5892−5901.
(21) Serafini, M. M.; Catanzaro, M.; Rosini, M.; Racchi, M.; Lanni, C. Curcumin in Alzheimer's disease: Can we think to new strategies and perspectives for this molecule? *Pharmacological research* **2017**, *124*, 146−155.
(22) Di Martino, R. M. C.; De Simone, A.; Andrisano, V.; Bisignano, P.; Bisi, A.; Gobbi, S.; Rampa, A.; Fato, R.; Bergamini, C.; Perez, D. I. Versatility of the curcumin scaffold: discovery of potent and balanced dual BACE-1 and GSK-3β inhibitors. *J. Med. Chem.* **2016**, *59* (2), 531−544.
(23) Konno, H.; Endo, H.; Ise, S.; Miyazaki, K.; Aoki, H.; Sanjoh, A.; Kobayashi, K.; Hattori, Y.; Akaji, K. Synthesis and evaluation of curcumin derivatives toward an inhibitor of beta-site amyloid precursor protein cleaving enzyme 1. *Bioorg. Med. Chem. Lett.* **2014**, *24* (2), 685−690.
(24) Sadegh Malvajerd, S.; Izadi, Z.; Azadi, A.; Kurd, M.; Derakhshankhah, H.; Sharifzadeh, M.; Akbari Javar, H.; Hamidi, M. Neuroprotective potential of curcumin-loaded nanostructured lipid carrier in an animal model of Alzheimer's disease: Behavioral and biochemical evidence. *J. Alzheimer's Dis.* **2019**, *69* (3), 671−686.
(25) Rahimi, H. R.; Nedaeinia, R.; Shamloo, A. S.; Nikdoust, S.; Oskuee, R. K. Novel delivery system for natural products: Nano-curcumin formulations. *Avicenna J. Phytomed.* **2016**, *6* (4), 383.
(26) Yang, K. Y.; Lin, L. C.; Tseng, T. Y.; Wang, S. C.; Tsai, T. H. Oral bioavailability of curcumin in rat and the herbal analysis from Curcuma longa by LC-MS/MS. *J. Chromatogr B Analyt Technol. Biomed Life Sci.* **2007**, *853* (1−2), 183−189.
(27) Gupta, T.; Singh, J.; Kaur, S.; Sandhu, S.; Singh, G.; Kaur, I. P. Enhancing bioavailability and stability of curcumin using solid lipid nanoparticles (CLEN): A covenant for its effectiveness. *Front. Bioeng. Biotechnol.* **2020**, *8*, 879.
(28) Kaminaga, Y.; Nagatsu, A.; Akiyama, T.; Sugimoto, N.; Yamazaki, T.; Maitani, T.; Mizukami, H. Production of unnatural glucosides of curcumin with drastically enhanced water solubility by cell suspension cultures of Catharanthus roseus. *FEBS letters* **2003**, *555* (2), 311−316.
(29) Pan, M.-H.; Huang, T.-M.; Lin, J.-K. Biotransformation of curcumin through reduction and glucuronidation in mice. *Drug metabolism and disposition* **1999**, *27* (4), 486−494.
(30) Feng, T.; Wei, Y.; Lee, R. J.; Zhao, L. Liposomal curcumin and its application in cancer. *International journal of nanomedicine* **2017**, *12*, 6027.
(31) Naksuriya, O.; Okonogi, S.; Schiffelers, R. M.; Hennink, W. E. Curcumin nanoformulations: a review of pharmaceutical properties and preclinical studies and clinical data related to cancer treatment. *Biomaterials* **2014**, *35* (10), 3365−3383.
(32) Zhang, J.; Wen, H.; Shen, F.; Wang, X.; Shan, C.; Chai, C.; Liu, J.; Li, W. Synthesis and biological evaluation of a novel series of curcumin-peptide derivatives as PepT1-mediated transport drugs. *Bioorganic Chemistry* **2019**, *92*, No. 103163.
(33) Wang, S.; Peng, X.; Cui, L.; Li, T.; Yu, B.; Ma, G.; Ba, X. Synthesis of water-soluble curcumin derivatives and their inhibition on lysozyme amyloid fibrillation. *Spectrochimica Acta Part A: Molecular and Biomolecular Spectroscopy* **2018**, *190*, 89−95.
(34) Dubey, S. K.; Sharma, A. K.; Narain, U.; Misra, K.; Pati, U. Design, synthesis and characterization of some bioactive conjugates of curcumin with glycine, glutamic acid, valine and demethylenated piperic acid and study of their antimicrobial and antiproliferative properties. *European journal of medicinal chemistry* **2008**, *43* (9), 1837−1846.
(35) Chyan, Y.-J.; Poeggeler, B.; Omar, R. A.; Chain, D. G.; Frangione, B.; Ghiso, J.; Pappolla, M. A. Potent neuroprotective properties against the Alzheimer β-amyloid by an endogenous melatonin-related indole structure, indole-3-propionic acid. *J. Biol. Chem.* **1999**, *274* (31), 21937−21942.
(36) Poeggeler, B.; Pappolla, M. A.; Hardeland, R.; Rassoulpour, A.; Hodgkins, P. S.; Guidetti, P.; Schwarcz, R. Indole-3-propionate: a potent hydroxyl radical scavenger in rat brain. *Brain research* **1999**, *815* (2), 382−388.
(37) Hwang, I. K.; Yoo, K. Y.; Li, H.; Park, O. K.; Lee, C. H.; Choi, J. H.; Jeong, Y. G.; Lee, Y. L.; Kim, Y. M.; Kwon, Y. G. Indole-3-propionic acid attenuates neuronal damage and oxidative stress in the ischemic hippocampus. *J. Neurosci. Res.* **2009**, *87* (9), 2126−2137.
(38) Li, Z.; Zhu, H.; Zhang, L.; Qin, C. The intestinal microbiome and Alzheimer's disease: A review. *Animal Models and Experimental Medicine* **2018**, *1* (3), 180−188.
(39) Sakayanathan, P.; Loganathan, C.; Kandasamy, S.; Ramanna, R. V.; Poomani, K.; Thayumanavan, P. In vitro and in silico analysis of novel astaxanthin-s-allyl cysteine as an inhibitor of butyrylcholinesterase and various globular forms of acetylcholinesterases. *Int. J. Biol. Macromol.* **2019**, *140*, 1147−1157.
(40) Benzie, I. F. F.; Strain, J. J. The ferric reducing ability of plasma (FRAP) as a measure of "antioxidant power": the FRAP assay. *Analytical biochemistry* **1996**, *239* (1), 70−76.
(41) Wang, X.; Zhang, T.; Chen, X.; Xu, Y.; Li, Z.; Yang, Y.; Du, X.; Jiang, Z.; Ni, H. Simultaneous Inhibitory Effects of All-Trans Astaxanthin on Acetylcholinesterase and Oxidative Stress. *Marine Drugs* **2022**, *20* (4), 247.
(42) Lineweaver, H.; Burk, D. The determination of enzyme dissociation constants. *Journal of the American chemical society* **1934**, *56* (3), 658−666.
(43) Dixon, M. The determination of enzyme inhibitor constants. *Biochemical journal* **1953**, *55* (1), 170.
(44) Cheung, J.; Rudolph, M. J.; Burshteyn, F.; Cassidy, M. S.; Gary, E. N.; Love, J.; Franklin, M. C.; Height, J. J. Structures of human acetylcholinesterase in complex with pharmacologically important ligands. *Journal of medicinal chemistry* **2012**, *55* (22), 10282−10286.
(45) Nicolet, Y.; Lockridge, O.; Masson, P.; Fontecilla-Camps, J. C.; Nachon, F. Crystal structure of human butyrylcholinesterase and of its complexes with substrate and products. *J. Biol. Chem.* **2003**, *278* (42), 41141−41147.
(46) Case, D. A.; Cheatham, T. E.; Darden, T.; Gohlke, H.; Luo, R.; Merz, K. M.; Onufriev, A.; Simmerling, C.; Wang, B.; Woods, R. J. The Amber biomolecular simulation programs. *J. Comput. Chem.* **2005**, *26* (16), 1668−1688.
(47) Götz, A. W.; Clark, M. A.; Walker, R. C. An extensible interface for QM/MM molecular dynamics simulations with AMBER. *J. Comput. Chem.* **2014**, *35* (2), 95−108.
(48) Hobza, P.; Hubalek, F.; Kabeláč, M.; Mejzlik, P.; Šponer, J.; Vondrášek, J. Ability of empirical potentials (AMBER, CHARMM, CVFF, OPLS, Poltev) and semi-empirical quantum chemical methods (AM1, MNDO/M, PM3) to describe H-bonding in DNA base pairs; comparison with ab initio results. *Chem. Phys. Lett.* **1996**, *257* (1−2), 31−35.
(49) *Gaussian 16 Rev. C.01*; Gaussian, Inc.: Wallingford, CT, 2016.
(50) Choudhary, V.; Bhatt, A.; Dash, D.; Sharma, N. DFT calculations on molecular structures, HOMO−LUMO study, reactivity descriptors and spectral analyses of newly synthesized diorganotin (IV) 2-chloridophenylacetohydroxamate complexes. *J. Comput. Chem.* **2019**, *40* (27), 2354−2363.
(51) Ashraf, N.; Asari, A.; Yousaf, N.; Ahmad, M.; Ahmed, M.; Faisal, A.; Saleem, M.; Muddassar, M. Combined 3D-QSAR, molecular docking and dynamics simulations studies to model and design TTK inhibitors. *Front. Chem.* **2022**, *10*, No. 1003816.
(52) Roe, D. R.; Cheatham, T. E., III PTRAJ and CPPTRAJ: software for processing and analysis of molecular dynamics trajectory data. *J. Comput. Theory Comput.* **2013**, *9* (7), 3084−3095.
(53) Abrahams, S.; Haylett, W. L.; Johnson, G.; Carr, J. A.; Bardien, S. Antioxidant effects of curcumin in models of neurodegeneration, aging, oxidative and nitrosative stress: A review. *Neuroscience* **2019**, *406*, 1−21.
(54) Ono, K.; Hasegawa, K.; Naiki, H.; Yamada, M. Curcumin has potent anti-amyloidogenic effects for Alzheimer's β-amyloid fibrils in vitro. *Journal of neuroscience research* **2004**, *75* (6), 742−750.

https://doi.org/10.1021/acsomega.4c08149
ACS Omega 2025, 10, 9073−9087

(55) Yin, W.; Zhang, X.; Li, Y. Protective effects of curcumin in APPswe transfected SH-SY5Y cells. *Neural Regen. Res.* **2012**, *7* (6), 405.
(56) Chin, D.; Huebbe, P.; Pallauf, K.; Rimbach, G. Neuroprotective properties of curcumin in Alzheimer's disease-merits and limitations. *Curr. Med. Chem.* **2013**, *20* (32), 3955−3985.
(57) Noureddin, S. A.; El-Shishtawy, R. M.; Al-Footy, K. O. Curcumin analogues and their hybrid molecules as multifunctional drugs. *European journal of medicinal chemistry* **2019**, *182*, No. 111631.
(58) Pandey, A.; Chaturvedi, M.; Mishra, S.; Kumar, P.; Somvanshi, P.; Chaturvedi, R. Reductive metabolites of curcumin and their therapeutic effects. *Heliyon* **2020**, *6* (11), No. e05469.
(59) Mishra, S.; Narain, U.; Mishra, R.; Misra, K. Design, development and synthesis of mixed bioconjugates of piperic acid−glycine, curcumin−glycine/alanine and curcumin−glycine−piperic acid and their antibacterial and antifungal properties. *Bioorganic & medicinal chemistry* **2005**, *13* (5), 1477−1486.
(60) Mishra, S.; Kapoor, N.; Ali, A. M.; Pardhasaradhi, B. V. V.; Kumari, A. L.; Khar, A.; Misra, K. Differential apoptotic and redox regulatory activities of curcumin and its derivatives. *Free Radical Biol. Med.* **2005**, *38* (10), 1353−1360.
(61) Parvathy, K. S.; Negi, P. S.; Srinivas, P. Curcumin−amino acid conjugates: synthesis, antioxidant and antimutagenic attributes. *Food Chem.* **2010**, *120* (2), 523−530.
(62) Harish, G.; Venkateshappa, C.; Mythri, R. B.; Dubey, S. K.; Mishra, K.; Singh, N.; Vali, S.; Bharath, M. M. S. Bioconjugates of curcumin display improved protection against glutathione depletion mediated oxidative stress in a dopaminergic neuronal cell line: implications for Parkinson's disease. *Bioorganic & medicinal chemistry* **2010**, *18* (7), 2631−2638.
(63) Dolai, S.; Shi, W.; Corbo, C.; Sun, C.; Averick, S.; Obeysekera, D.; Farid, M.; Alonso, A.; Banerjee, P.; Raja, K. Clicked" sugar−curcumin conjugate: modulator of amyloid-β and tau peptide aggregation at ultralow concentrations. *ACS chemical neuroscience* **2011**, *2* (12), 694−699.
(64) Poeggeler, B.; Sambamurti, K.; Siedlak, S. L.; Perry, G.; Smith, M. A.; Pappolla, M. A. A novel endogenous indole protects rodent mitochondria and extends rotifer lifespan. *PLoS One* **2010**, *5* (4), No. e10206.
(65) Pappolla, M. A.; Perry, G.; Fang, X.; Zagorski, M.; Sambamurti, K.; Poeggeler, B. Indoles as essential mediators in the gut-brain axis. Their role in Alzheimer's disease. *Neurobiology of disease* **2021**, *156*, No. 105403.
(66) Kalaycıoğlu, Z.; Gazioğlu, I.; Erim, F. B. Comparison of antioxidant, anticholinesterase, and antidiabetic activities of three curcuminoids isolated from Curcuma longa L. *Natural Product Research* **2017**, *31* (24), 2914−2917.
(67) Akinyemi, A. J.; Oboh, G.; Fadaka, A. O.; Olatunji, B. P.; Akomolafe, S. Curcumin administration suppress acetylcholinesterase gene expression in cadmium treated rats. *Neurotoxicology* **2017**, *62*, 75−79.
(68) Ahmed, T.; Gilani, A.-H. Inhibitory effect of curcuminoids on acetylcholinesterase activity and attenuation of scopolamine-induced amnesia may explain medicinal use of turmeric in Alzheimer's disease. *Pharmacol., Biochem. Behav.* **2009**, *91* (4), 554−559.
(69) Jiang, H.; Chen, C.; Gao, J. Extensive Summary of the Important Roles of Indole Propionic Acid, a Gut Microbial Metabolite in Host Health and Disease. *Nutrients* **2023**, *15* (1), 151.
(70) Reyes, A. E.; Chacón, M. A.; Dinamarca, M. C.; Cerpa, W.; Morgan, C.; Inestrosa, N. C. Acetylcholinesterase-Aβ complexes are more toxic than Aβ fibrils in rat hippocampus: effect on rat β-amyloid aggregation, laminin expression, reactive astrocytosis, and neuronal cell loss. *American journal of pathology* **2004**, *164* (6), 2163−2174.
(71) Bartolini, M.; Bertucci, C.; Cavrini, V.; Andrisano, V. β-Amyloid aggregation induced by human acetylcholinesterase: inhibition studies. *Biochemical pharmacology* **2003**, *65* (3), 407−416.
(72) García-Ayllón, M.-S.; Small, D. H.; Avila, J.; Sáez-Valero, J. Revisiting the role of acetylcholinesterase in Alzheimer's disease: cross-talk with P-tau and β-amyloid. *Front. Mol. Neurosci.* **2011**, *4*, 22.
(73) Inestrosa, N. C.; Sagal, J. P.; Colombres, M. Acetylcholinesterase interaction with Alzheimer amyloid β. In *Alzheimer's Disease: Cellular and Molecular Aspects of Amyloid β*; Springer: Boston, MA, 2005; pp. 299−317.
(74) Weinstock, M. Selectivity of cholinesterase inhibition: clinical implications for the treatment of Alzheimer's disease. *CNS drugs* **1999**, *12* (4), 307−323.
(75) Kandiah, N.; Pai, M.-C.; Senanarong, V.; Looi, I.; Ampil, E.; Park, K. W.; Karanam, A. K.; Christopher, S. Rivastigmine: the advantages of dual inhibition of acetylcholinesterase and butyrylcholinesterase and its role in subcortical vascular dementia and Parkinson's disease dementia. *Clin. Intervent. Aging* **2017**, *12*, 697−707.
(76) Stavrakov, G.; Philipova, I.; Lukarski, A.; Atanasova, M.; Zheleva, D.; Zhivkova, Z. D.; Ivanov, S.; Atanasova, T.; Konstantinov, S.; Doytchinova, I. Galantamine-curcumin hybrids as dual-site binding acetylcholinesterase inhibitors. *Molecules* **2020**, *25* (15), 3341.
(77) Pietrucci, F. Strategies for the exploration of free energy landscapes: Unity in diversity and challenges ahead. *Rev. Phys.* **2017**, *2*, 32−45.
(78) Saravanan, K.; Kalaiarasi, C.; Kumaradhas, P. Understanding the conformational flexibility and electrostatic properties of curcumin in the active site of rhAChE via molecular docking, molecular dynamics, and charge density analysis. *J. Biomol. Struct. Dyn.* **2017**, *35* (16), 3627−3647.
(79) LoPachin, R. M.; Geohagen, B. C.; Nordstroem, L. Mechanisms of soft and hard electrophile toxicities. *Toxicology* **2019**, *418*, 62−69.

https://doi.org/10.1021/acsomega.4c08149
ACS Omega 2025, 10, 9073−9087